Acta Crystallographica Section D
Biological Crystallography
ISSN 0907-4449

Structures of human MST3 kinase in complex with adenine, ADP and Mn^{2+}

Tzu-Ping Ko,[a]‡ Wen-Yih Jeng,[a,b]‡ Chia-I Liu,[a,b,c] Ming-Derg Lai,[d] Chun-Lan Wu,[a,b] Wei-Jung Chang,[a,b] Hui-Lin Shr,[a,b] Te-Jung Lu[e] and Andrew H.-J. Wang[a,b,c]*

[a]Institute of Biological Chemistry, Academia Sinica, Taipei 115, Taiwan, [b]Core Facility for Protein Production and X-ray Structural Analysis, Academia Sinica, Taipei 115, Taiwan, [c]Institute of Biochemical Sciences, National Taiwan University, Taipei 106, Taiwan, [d]Department of Biochemistry and Molecular Biology, College of Medicine, National Cheng Kung University, Tainan 701, Taiwan, and [e]Department of Medical Technology, Chung Hwa University of Medical Technology, Tainan 717, Taiwan

‡ These authors contributed equally.

Correspondence e-mail: ahjwang@gate.sinica.edu.tw

Received 28 September 2009
Accepted 10 November 2009

PDB References: MST3 kinase domain, unliganded, crystal form I, 3a7f; form II, 3a7g; ADP complex, 3a7h; Mn-ADP complex, 3a7j; form III adenine complex, 3a7i.

The MST family is a subclass of mammalian serine/threonine kinases that are related to the yeast sterile-20 protein and are implicated in regulating cell growth and transformation. The MST3 protein contains a 300-residue catalytic domain and a 130-residue regulatory domain, which can be cleaved by caspase and activated by autophosphorylation, promoting apoptosis. Here, five crystal structures of the catalytic domain of MST3 are presented, including a complex with ADP and manganese, a unique cofactor preferred by the enzyme, and a complex with adenine. Similar to other protein kinases, the catalytic domain of MST3 folds into two lobes: the smaller N lobe forms the nucleotide-binding site and the larger C lobe recognizes the polypeptide substrate. The bound ADP and Mn^{2+} ions are covered by a glycine-rich loop and held in place by Asn149 and Asp162. A different orientation was observed for the ligand in the MST3–adenine complex. In the activation loop, the side chain of Thr178 is phosphorylated and is sandwiched by Arg143 and Arg176. Comparison of this structure with other similar kinase structures shows a 180° rotation of the loop, leading to activation of the enzyme. The well defined protein–ligand interactions also provide useful information for the design of potent inhibitors.

1. Introduction

Ser/Thr protein kinases, which transfer the γ-phosphate group of ATP (or GTP) to the hydroxyl group of a serine or threonine side chain, represent a major class of cellular regulators of protein activity. They have been classified into six large groups, among which are the AGC group, which includes the cAMP-dependent protein kinase A (PKA), and the STE group, which includes homologues of the yeast sterile-20 (ste20) protein (Goldsmith *et al.*, 2007). Although the molecular architectures and regulation mechanisms differ greatly among these enzymes, they all contain a two-lobe core catalytic domain (Johnson *et al.*, 2001). The smaller N-terminal lobe forms the ATP-binding site and the larger C-terminal lobe recognizes the protein substrate and participates in the phosphorylation reaction. In general, the phosphorylation of a key Ser/Thr residue in the activation loop is essential for the activity of the enzyme, which is controlled by the conformation of this loop (Nolen *et al.*, 2004).

The complex structure of the catalytic (C) and regulatory (R) subunits led to the elucidation of the control mechanism

of PKA (Kim *et al.*, 2005). Upon binding cAMP, the R subunit undergoes conformational changes and releases the activation loop of the bound C subunit. A *trans* phosphorylation/activation mechanism was suggested from the crystal structures of human Chk2 (checkpoint kinase 2), SLK (ste20-like kinase), LOK (lymphocyte-originated kinase) and DAPK3 (death-associated protein kinase 3), which showed the formation of dimers by exchanging activation loops (Oliver *et al.*, 2007; Pike *et al.*, 2008). In contrast, the structures of PAK1 (p21-activated kinase 1, an STE-group enzyme) and MEK1/2 and 6 (MAP/ERK kinases, mitogen-activated enzymes) showed dimers in which the activation loop appeared to be auto-inhibitory (Lei *et al.*, 2000; Ohren *et al.*, 2004; Min *et al.*, 2009).

MST3, which was first characterized by Schinkmann & Blenis (1997) and is also known as STK24, is an upstream mammalian ste20-like kinase belonging to the germinal centre kinase (GCK) subclass of the STE-group enzymes (Ling *et al.*, 2008). The MST family of protein kinases play a critical role in the regulation of cell death in diverse organisms including mammals. MST1 is activated by oxidative stress and phosphorylates the transcription factor FOXO3, leading to disruption of the interactions between FOXO3 and 14-3-3 proteins and the accumulation of FOXO3 in the nucleus, where FOXO3 induces the expression of cell-death genes (Lehtinen *et al.*, 2006). In nematodes, the MST1 orthologue CST-1 extends the life span of *Caenorhabditis elegans* (Lehtinen *et al.*, 2006). Each MST protein is comprised of an N-terminal catalytic domain and a C-terminal regulatory domain. An intact C-terminal domain is required for MST1 (and possibly MST2) dimerization, whereas it remains uncertain whether MST3 and MST4 also form dimers (Ling *et al.*, 2008). MST3 shows a unique cofactor preference towards manganese ions, although it can use other divalent ions as the cofactor and GTP as the phosphate donor in kinase reactions (Schinkmann & Blenis, 1997; Lu *et al.*, 2006). MST activity can be regulated by caspase-induced cleavage as well as by interactions with other intracellular proteins (Huang *et al.*, 2002; Lehtinen & Bonni, 2008).

To better understand the regulation mechanism of MST3 and of the MST-family kinases in general, we expressed recombinant MST3 in *Escherichia coli* either as a full-length protein (431 amino acids) or truncated at various sites in the C-terminal domain. Crystals of MST3(1–303), which contained residues 1–303 and encompassed the catalytic domain but lacked the regulatory domain, were obtained in three different unit cells. In all crystal forms, the protein turned out to be a monomer, with the key residue Thr178 in the activation loop being phosphorylated. The structures observed in these crystals included a complex with ADP and manganese ions and a complex with an adenine bound to the active site. Comparison of the MST3(1–303) structure with those of similar kinases suggests that the phosphorylation of Thr178 accounts for the prominent conformational differences in the activation loop. Furthermore, the detailed enzyme–ligand interactions provided by the crystal structures might find use in the design of specific inhibitors against this family of cell-death-related kinases.

2. Materials and methods

2.1. Expression of the *mst3* gene and purification of the MST3 protein

Gene fragments for the N-terminal catalytic domain of MST3 (1–303) and full-length MST3 (1–431) were amplified directly from the cDNA of full-length MST3 (Lu *et al.*, 2006) by polymerase chain reaction (PCR) with forward primer 5′-GGTATTGAGGGTCGCATGGCTCACTCCCCGGTG-3′ and reverse primer 5′-AGAGGAGAGTTAGAGCCTTACG-AGTCGTCATGGCTCTGC-3′ (for the catalytic domain) or 5′-AGAGGAGAGTTAGAGCCTCAGTGGGATGAAGTT-CCTC-3′ (for the full-length protein). The PCR products encoding MST3 were cloned into the expression vector pET-32 Xa/LIC (Novagen), which contained a thioredoxin-coding region. All DNA constructs were verified by nucleotide sequencing. The correct constructs were transformed into *E. coli* ArcticExpress (DE3) competent cells (Stratagene) for protein expression.

An overnight culture of a single transformant (100 ml) was inoculated into 6 l fresh LB medium containing 100 µg l^{-1} ampicillin, which was subsequently incubated at 303 K until the medium reached an $A_{600\,\mathrm{nm}}$ of 0.8–1.0. The temperature was then reduced to 286 K and the bacteria were allowed to cool for 1 h before adding the inducer isopropyl β-D-1-thio-galactopyranoside to a final concentration of 1 m*M*. After further growth for 16 h at 286 K, the bacterial cells were harvested by centrifugation at 7000*g* and immediately resuspended in lysis buffer containing 20 m*M* Tris–HCl, 400 m*M* NaCl, 10 m*M* imidazole pH 7.5. The cells were then broken using a Cell Disruption System (Constant Systems Ltd, UK) and the cell debris was removed by centrifugation at 17 000*g*.

The cell-free extract was loaded onto an Ni^{2+}–NTA column which had been equilibrated with lysis buffer. The column was washed using the same buffer and the thioredoxin-fused MST3 protein was subsequently eluted with a linear gradient of 10–300 m*M* imidazole. After checking by SDS–PAGE, the eluted fractions containing the MST3 protein were pooled and treated with factor Xa (Novagen) to cleave the MST3 from the polyhistidine-containing N-terminal thioredoxin-fusion tag. The thioredoxin tag and the tag-free MST3 were then separated using a second Ni^{2+}–NTA column. The tag-free MST3 was dialyzed against a buffer containing 100 m*M* NaCl, 10% glycerol and 50 m*M* Tris–HCl pH 8.0 to remove imidazole and was concentrated using a 10 kDa cutoff Amicon Ultra-15 (Millipore, Massachusetts, USA) before storage at 193 K. The plasmids for the MST3 mutants (T178A and T178E) were prepared using a QuikChange site-directed mutagenesis kit (Stratagene) and the proteins were expressed and purified following the same procedures as used for the wild-type MST3. The protein solutions might contain small amounts of factor Xa.

2.2. Crystallization and structure determination

The purified MST3(1–303) protein was crystallized using the vapour-diffusion method (McPherson, 1999), employing sitting-drop plates in conjunction with various screening kits

Table 1
Data-collection and refinement statistics for the crystals of MST3.

All positive reflections were used in the refinement. Values in parentheses are for the highest resolution shells. The phosphate attached to Thr178 is counted as protein and the Mn ions as ligands.

	Type I (native)	Type II (native)	Type II (ADP)	Type III (adenine)	Type III (ADP + Mn)
Data collection					
Space group	*C*2	$P2_1$	$P2_1$	$P2_1$	$P2_1$
Unit-cell parameters					
a (Å)	99.14	55.79	55.68	47.58	47.82
b (Å)	59.26	95.02	95.19	55.60	53.57
c (Å)	61.54	61.37	61.48	60.48	60.63
β (°)	93.71	93.36	93.45	111.13	109.95
Resolution (Å)	30–1.55 (1.61–1.55)	20–2.00 (2.07–2.00)	20–1.96 (2.03–1.96)	30–1.45 (1.50–1.45)	30–1.50 (1.55–1.50)
Unique reflections	51285 (5146)	42786 (4282)	45166 (4541)	50491 (5083)	45787 (4543)
Redundancy	5.5 (5.4)	4.6 (4.5)	5.0 (4.5)	4.2 (4.1)	5.0 (4.7)
Completeness (%)	99.1 (99.7)	99.7 (100.0)	99.2 (99.8)	97.0 (98.2)	99.0 (99.4)
Average $I/\sigma(I)$	50.2 (3.0)	35.9 (5.8)	49.2 (5.5)	45.7 (2.6)	40.2 (4.5)
$R_{\rm merge}$ (%)	3.0 (52.7)	4.1 (35.2)	3.9 (37.5)	3.2 (48.3)	3.8 (34.6)
Refinement					
No. of protein molecules	1	2	2	1	1
No. of reflections	49374 (4520)	41607 (3747)	43940 (3800)	48955 (4382)	44208 (4027)
$R_{\rm work}$ (95% of data)	0.195 (0.261)	0.199 (0.280)	0.204 (0.287)	0.187 (0.276)	0.186 (0.248)
$R_{\rm free}$ (5% of data)	0.219 (0.294)	0.247 (0.309)	0.252 (0.318)	0.217 (0.312)	0.210 (0.283)
R.m.s.d. bond distance (Å)	0.020	0.021	0.020	0.019	0.019
R.m.s.d. bond angle (°)	2.0	2.0	1.9	1.9	2.0
Ramachandran plot (%)					
Most favoured regions	90.2	88.6	89.8	89.7	90.5
Additional allowed regions	9.0	10.4	9.1	9.5	8.3
Other regions	0.8	1.0	1.0	0.8	1.2
No. of non-H atoms					
Protein	2271	4644	4644	2302	2302
Water	321	461	476	417	383
Ligand			54	10	29
Average *B* (Å^2)					
Protein	30.6	44.3	43.1	28.5	24.6
Water	39.8	53.6	52.3	43.6	38.6
Ligand			64.3	30.4	25.7

(Hampton Research). Crystallization of MST3(1–303) in the first unit cell (*C*2; type I) was carried out by mixing equal volumes (2 µl) of protein solution [60 mg ml^{-1} MST3(1–303) in 50 m*M* Tris–HCl pH 8.0, 100 m*M* NaCl, 10%(*v*/*v*) glycerol and 5 m*M* dithiothreitol] and reservoir solution [0.1 *M* Tris–HCl pH 8.5, 0.4 *M* sodium formate and 10%(*w*/*v*) PEG 4000] and equilibrating against 250 µl reservoir solution. The other two crystal forms ($P2_1$; type II and type III) were obtained by reducing the protein concentration to 25 mg ml^{-1} in the same buffer and using a reservoir consisting of 0.1 *M* Tris–HCl pH 8.5, 200 m*M* $MgCl_2$ and 13%(*w*/*v*) PEG 3350. Type II crystals with bound ligand were obtained by adding 1 µl reservoir solution containing 100 m*M* ATP to the sitting drop and soaking for 2 h. Either 10 m*M* ATP or 10 m*M* ADP was added to the protein solution of type III crystals, while the reservoir for the Mn-ADP complex contained 180 m*M* $MgCl_2$ and 5 m*M* manganese acetate instead of 200 m*M* $MgCl_2$. Some mutant proteins were found to crystallize in $P2_1$ unit cells (type II and III) under similar conditions. Attempts to crystallize full-length MST3 were unsuccessful.

X-ray diffraction data were collected at cryogenic temperatures from 20 wild-type and two mutant crystals using synchrotron radiation at SPring-8 and Photon Factory in Japan and NSRRC in Taiwan. Prior to flash-freezing, the crystals were soaked briefly in reservoir solution containing the appropriate ligands and 15% glycerol as a cryoprotectant. The diffraction images were processed using *HKL*-2000 (Otwinowski & Minor, 1997). The statistics for five representative data sets are shown in Table 1.

Several protein kinase catalytic domains from the PDB, including 1f3m (Lei *et al.*, 2000), 1yhv (Lei *et al.*, 2005) and 2j7t (Pike *et al.*, 2008), were tried as search models for determination of the MST3(1–303) structure by the molecular-replacement method. The 'native' structure of the type I crystal was solved using a monomer of 2j7t. Despite an initial *R* value of 0.53 at 2.0 Å, the Fourier maps (FOM = 0.32) showed good electron density for the polypeptide backbone as well as most side chains. An exception was the region containing residues 166–196, which corresponds to the activation loop. This loop was tentatively deleted, but most of it was rebuilt in later stages of refinement according to the improved densities. It turned out to be a major region of conformational change in MST3 when compared with the 2j7t model. The structures of the type II and type III crystals were determined by molecular replacement using the refined native model of the type I crystal.

All crystallographic computations were carried out using the program *CNS* (Brünger *et al.*, 1998); manual model building used the program *O* (Jones *et al.*, 1991) and molecular graphics were produced using *PyMOL* (DeLano, 2008).

3. Results

3.1. Overall structure

The structure of MST3(1–303) was initially determined in a monoclinic *C*2 unit cell (type I crystal) by molecular-replacement methods using PDB entry 2j7t as a search model, which contained the catalytic domain of human LOK (Pike *et al.*, 2008). The *C*2 model was then used to solve the structures of two other crystal forms (types II and III), both of which belonged to space group $P2_1$, but one of which had a unit cell that was twice as large as the other (Table 1). In addition to the unliganded protein, we also included ADP, ATP or its analogue AMPPNP (in which the O atom connecting the β- and γ-phosphates is replaced by N) and the metal ions Mn^{2+},

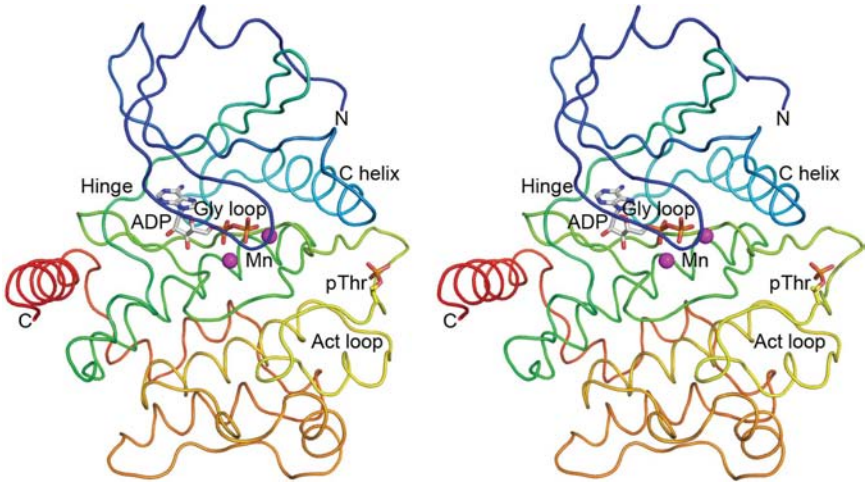

Figure 1
Structure of the MST3 catalytic domain. A molecule of MST3(1–303) is shown as a backbone trace from the N-terminus to the C-terminus, colour coded by a spectrum from blue to red. The protein adopts a typical protein kinase fold, which consists of an N lobe (blue–cyan) and a C lobe (green–yellow–red) connected by a hinge. The bound ADP and two Mn^{2+} ions in this representative structure are shown as sticks and balls, respectively, as is the phosphorylated side chain of Thr178 (pThr). The locations of the glycine-rich loop (Gly loop), the C helix, the hinge and the activation loop (Act loop) are labelled.

Mg^{2+} or Zn^{2+} (as cofactors) in the crystallization solution. Upon preliminary analysis (see Table S1 in the Supplementary Material[1]), five of the 21 data sets collected from the various crystals stood out as the best data sets and were used in subsequent refinements. Some statistical data for these models can be found in Table 1. The quality of the models can be inferred from the collection of high-resolution data to beyond 1.5 Å, the low R_{work} and R_{free} values (with an R_{free} of about 30% for the outermost shells) and the distribution of peptide dihedral angles (90% lying inside the core regions). Asp92 and Arg143 have special conformations of (φ, ψ) = (60°, −120°) and (60°, 0°). Asp92 is located in a β-turn where a glycine is usually found (Richardson, 1981). Arg143 occurs at the C-terminal end of a short β-strand and is functionally important (see below).

As shown in Fig. 1, the catalytic domain of MST3 adopts the typical two-lobe protein kinase fold with an approximately 100-residue N-terminal lobe (N lobe) and a 200-residue C-terminal lobe (C lobe); these are comprised principally of a β-barrel and several α-helices, respectively, and are connected by a hinge. Excluding the regions of largest conformational difference, models of the entire catalytic domain can be superimposed on one another with root-mean-square deviations (r.m.s.d.s) of 0.27–1.30 Å for 268–291 C^{α} atoms (Table S2[1]) using the least-squares fitting protocol of the program *O* (Jones *et al.*, 1991) with a matching criterion of 3.8 Å. In general, the N lobe shows greater structural differences than the C lobe. When superimposed separately, the N-lobe models differed by r.m.s.d.s of 0.32–1.31 Å and the C-lobe models by 0.14–0.44 Å (Table S3[1]). The N-terminal region of the third crystal form (type III) does not superimpose with those of the other two crystal forms (types I and II). Interestingly, the models differ from one another in the relative dispositions of the two lobes. The largest difference corresponds to a rotation of nearly 12° (Table S2[1]) about the hinge of three consecutive glycines 103–105. Prominent structural variations also occur in another glycine-rich region 31–36 (G*x*G*xx*G, termed the glycine-rich loop), which covers the phosphate moiety of ATP during catalysis (Johnson *et al.*, 2001), and in the important C helix (Fig. 2).

The structures of MST3(1–303) presented here show r.m.s.d.s of 0.56–1.07 Å for 252–276 C^{α} atoms from those of PDB entries 3ckw and 3ckx (Table S4[1]), which contain the catalytic domain of MST3 crystallized in a unit cell similar to that of our type III crystal. 3ckw and 3ckx (S. S. Antonysamy, S. K. Burley, S. Buchanan, F. Chau, I. Feil, L. Wu & J. M. Sauder, unpublished work) differed by 0.76 Å for 255 C^{α} atoms. The models of PDB entry 3com (S. Atwell, S. K. Burley, M. Dickey, B. Leon & J. M. Sauder, unpublished work), which contains the MST1 catalytic domain, showed r.m.s.d.s of 1.01–1.55 Å for 243–268 C^{α} atoms when compared with MST3(1–303) (Table S4[1]). Other structural features of MST3(1–303) are detailed in the following.

3.2. The active conformation of MST3

The native *C*2 crystal (type I) contains one MST3(1–303) molecule in the asymmetric unit, the first $P2_1$ crystal (type II) contains two molecules and the second $P2_1$ crystal (type III) contains one molecule. The *C*2 structure encompasses amino-acid residues 9–169 and 176–298, with part of the activation loop being disordered. In the $P2_1$ crystals (types II and III), the polypeptide chains are continuous but they also lack the N- and C-termini, which are exposed to the bulk solvent. The key residue Thr178 is phosphorylated, as clearly seen in the type III crystals, but the electron density corresponding to the phosphate moiety is weak in the type I and type II crystals. In fact, the average temperature factor (*B* value) of the phosphorylated Thr178 (pThr178) in the *C*2 crystal is 53 $Å^2$, which is significantly higher than the overall protein *B* value of 31 $Å^2$. In the native type II crystal, the *B* value of pThr178 is also high at 76 $Å^2$ compared with the overall value of 44 $Å^2$, despite the entire activation loop being visible in the electron-density map. In the activation loop of all MST3(1–303) structures the phosphate group of pThr178 is sandwiched by the two positively charged side chains of Arg143 and Arg176 (Fig. 3*a*). In the two unliganded structures, the *B* values of Arg176 (50 and 86 $Å^2$ in type I and type II crystals, respectively) are also high, whereas those of Arg143 (35 and 43 $Å^2$,

[1] Supplementary material has been deposited in the IUCr electronic archive (Reference: MV5032). Services for accessing this material are described at the back of the journal.

respectively) are comparable to the overall protein average. The other type II crystal with a bound ligand appears to be a similar case, but in the type III crystals the *B* values of Arg176 and Thr178 (both about 26 Å^2) are actually lower than the overall *B* value of 28 Å^2. Because Arg176 is located adjacent to Thr178 and their motility may be correlated, it is likely that the variable *B* values are a consequence of flexibility of the activation loop rather than partial phosphorylation.

With a special α_L-like conformation, Arg143 of MST3 terminates a short β-strand (β6) and is equivalent to Arg165 of PKA (Johnson *et al.*, 2001). In addition to pThr178, its side chain binds to the side-chain O$^{\eta}$ atom of Tyr196, which further forms a hydrogen bond to the backbone O atom of pThr178 (Fig. 3*a*). A similar hydrogen-bond network has been observed in other structures, including PAK (Eswaran *et al.*, 2007). The adjacent Asp144 serves as the catalytic base in the phosphate-transfer reaction (Johnson *et al.*, 2001). Because activation of MST3 depends on the phosphorylation of Thr178, the special peptide conformation of Arg143 is probably essential for the function of the enzyme since it mediates communication between the activation loop and the active site. The strand β6 immediately follows the major helix αE and forms an antiparallel ribbon with another short strand β9, which constitutes the first secondary-structural element in the activation loop (Fig. 3*b*). In the model of LOK (PDB entry 2j7t, which was used in molecular replacement), the corresponding region is part of an α-helix denoted αAL (Pike *et al.*, 2008). Strand β9 is preceded by the conserved DFG motif that contains Asp162, which is important for binding to cofactor metal ions. It is succeeded by a short turn and a stretch of peptide (corresponding to the rest of helix αAL in LOK) that connects to Thr178.

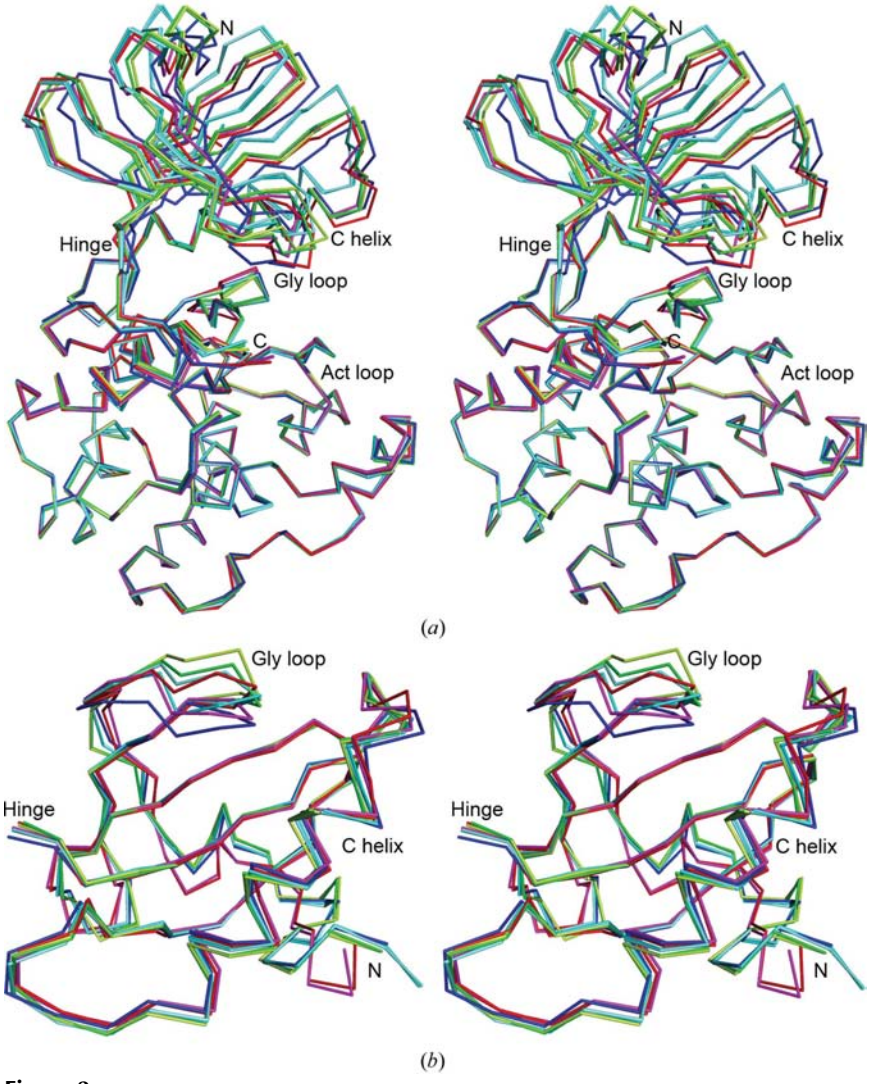

Figure 2
Comparison of MST3(1–303) models. (*a*) The seven crystallographically independent structures are superimposed on the basis of C$^{\alpha}$ positions in the C lobe. The significant conformational variations in the N lobe, as illustrated here in a slightly different view from Fig. 1, can be attributed to rigid-body rotations anchored at the hinge and roughly about a line extending from the hinge to the C-terminal end of the C helix. (*b*) The models of the N lobe are superimposed and viewed approximately through the inter-lobal interface. Although most of the C$^{\alpha}$ atoms are well matched, deviations in the N-terminal region, including the glycine-rich loop, are prominent. The model of the native type I crystal is shown in blue, those of the native type II crystals are shown in lemon and cyan, the type II–ADP models are shown in green and aquamarine, the type III–adenine model is shown in magenta and the type III–Mn-ADP model is shown in red.

Interestingly, despite the apparent structural disparity in the activation loop, the entire segment of Val180–Gln193 in MST3 superimposes very well with Ile193–Cys206 in LOK, with r.m.s.d.s of 0.34–0.43 Å for the 14 C$^{\alpha}$ positions. The movement entails a rotation of 176–179° with respect to the other part of the kinase molecule (Fig. 3*c*). In fact, the rotation axis coincides with the molecular dyad of the LOK dimer (Fig. 3*d*), in which the activation loops are reciprocally exchanged between the monomers (Oliver *et al.*, 2007; Pike *et al.*, 2008). This 14-residue segment begins with a short region that assumes an extended (β-like) peptide conformation and encompasses the P+1 loop and helix αEF (Nolen *et al.*, 2004). It buries an average surface area of 806 Å^2 of the MST3(1–303) molecule with residues Asp162–Ala195 omitted. In addition to the hydrophobic interactions between a number of nonpolar side chains (Fig. 3*e*), some specific hydrogen bonds in this region include (i) the side-chain O$^{\gamma1}$ atom of Thr182 to Asp144 O$^{\delta1}$ and Lys146 N$^{\zeta}$, mediating their charge–charge interaction, (ii) Trp185 N$^{\varepsilon1}$ to Glu211 O$^{\varepsilon1}$ and (iii) Glu189 O$^{\varepsilon1}$ and O$^{\varepsilon2}$ to Arg262 N$^{\eta1}$ and N$^{\eta2}$, forming a bidentate salt bridge. The aforementioned Tyr196 marks the division between helix αEF and another major helix αF. With proper accommodation of the core segment in its binding pocket, the network of interactions (Arg143, Arg176, pThr178,

Tyr196 *etc*.) and other anchoring mechanisms common to most protein kinases (Nolen *et al.*, 2004) ensure the correct formation of the activation loop, which endows the enzyme with full activity.

3.3. The ATP binding site

Although no nucleotide or cofactor was included when the native MST3(1–303) protein was crystallized, its active-site region turned out not to be entirely empty. In other known kinase structures this site is frequently occupied by a bound ATP, ADP or drug ligand, including substituted purines. When the protein was expressed in *E. coli*, some ligand might have been trapped in the active site and copurified with the enzyme. However, because the corresponding electron densities were weak in our native crystals, they could only be modelled as solvent molecules. Crystals containing bound ligands were subsequently obtained by soaking the type II crystals with ATP or by cocrystallization of the type III crystals with ATP and ADP.

Each MST3(1–303) molecule in the ATP-soaked type II crystal contained an ADP molecule (but not ATP) bound to the active site (Fig. 4*a*). Some electron density adjacent to the β-phosphate was modelled as a water molecule because we were not certain whether it corresponded to the γ-phosphate or a metal ion. This density can also be assigned to an alternative position occupied by the α-phosphate when a fraction of the bound ADP molecules adopt a similar conformation as observed in the type III crystals of the Mn-ADP complex (see below; Fig. S1). Either the ATP was hydrolyzed to ADP during the 2 h soaking time or the γ-phosphate was not bound properly and was consequently disordered. The average *B*

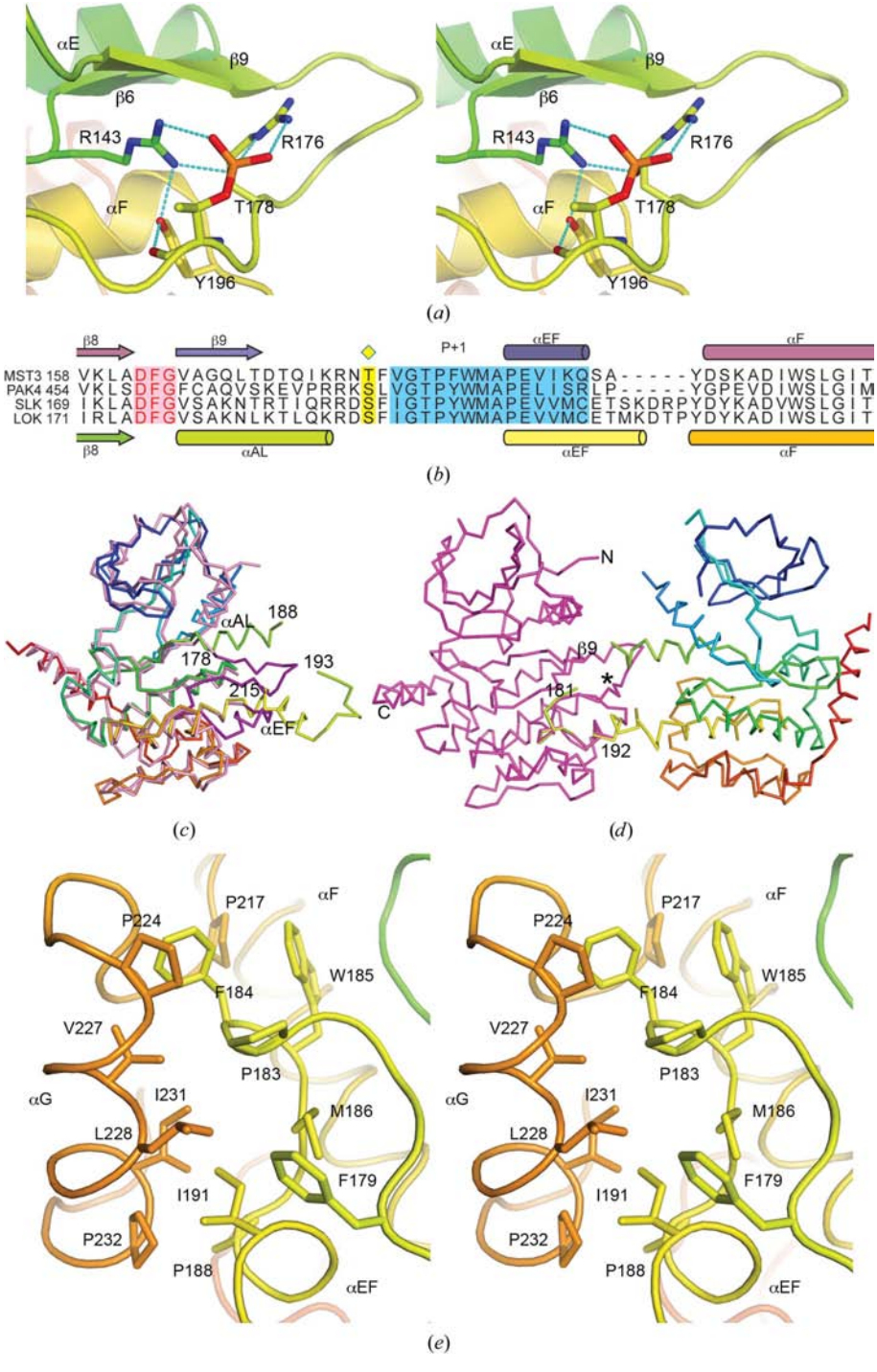

Figure 3
Molecular switch for the active conformation. (*a*) Hydrogen bonds centred at pThr178 stabilize the activation loop. In addition to the network involving the side chains of Arg143, Arg176 and Tyr196, this region also features the juxtaposition of the antiparallel strands β6 and β9. (*b*) The amino-acid sequence in the activation-loop region of MST3 is aligned with those of PAK4, SLK and LOK. The conserved DFG motif, the key Ser/Thr residue for phosphorylation and the 14-residue segment are coloured pink, yellow and blue, respectively. Cylinders and arrows indicate α-helices and β-strands observed in the MST3 (above) and LOK (below) structures. (*c*) Superposition of the MST3 and LOK monomers shows that the segment consisting of P+1 and αEF is related by a nearly 180° rotation. The C^{α} tracing of MST3 is shown in pink, with the activation loop highlighted in purple. That of LOK is colour-coded from the N-terminus (blue) to the C-terminus (red). Some of the LOK residues are labelled, as well as the locations of the helices αAL and αEF. (*d*) When MST3 and LOK are superimposed the other way, by the 14-residue segment, the resultant models are similar to a LOK dimer. MST3 is shown in magenta and LOK is coloured as in (*c*). The numbering is that for MST3 and the locations of secondary-structural conversion (β9) and the phosphorylation site (asterisk) are also labelled. (*e*) In MST3, the segment consisting of P+1 and αEF is packed against helix αG with several nonpolar side chains involved in hydrophobic interactions.

value of the ligands (64 Å^2) in the refined model is much higher than that of the protein (43 Å^2; Table 1).

The ligands have similar conformations in the two crystallographically independent MST3(1–303) molecules despite the conformational difference of the enzyme corresponding to a rotation of about 8° in the overall arrangement of the N lobe with respect to the C lobe. The two ADP molecules match better when the entire protein models are superimposed than when the individual lobes are used. Each ADP molecule appears to attach to the hinge between the two lobes through hydrogen bonding to its adenine base (Fig. 4*a*). Hydrophobic interactions between the purine ring and the nonpolar side chains of Ile30, Val38, Ala51 and Met99 from the N lobe and Leu151 from the C lobe further stabilize the enzyme–ligand complex. On the other hand, the sugar-phosphate moiety is less ordered than the adenine moiety, as reflected in the *B*-value difference of 20–30 Å^2 between the adenine and the phosphate groups. The ribose is not in direct contact with any protein atoms, whereas the α-phosphate makes a hydrogen bond to Lys53 and the β-phosphate makes a possible hydrogen bond to Asp162. The pyrophosphate is 4 Å away from the glycine-rich loop, sustaining meagre interactions. Despite the presence of $MgCl_2$ in the crystallization mother liquor, no Mg^{2+} ions were observed in this ADP-complex crystal or in any other type II crystals obtained using similar soaking techniques.

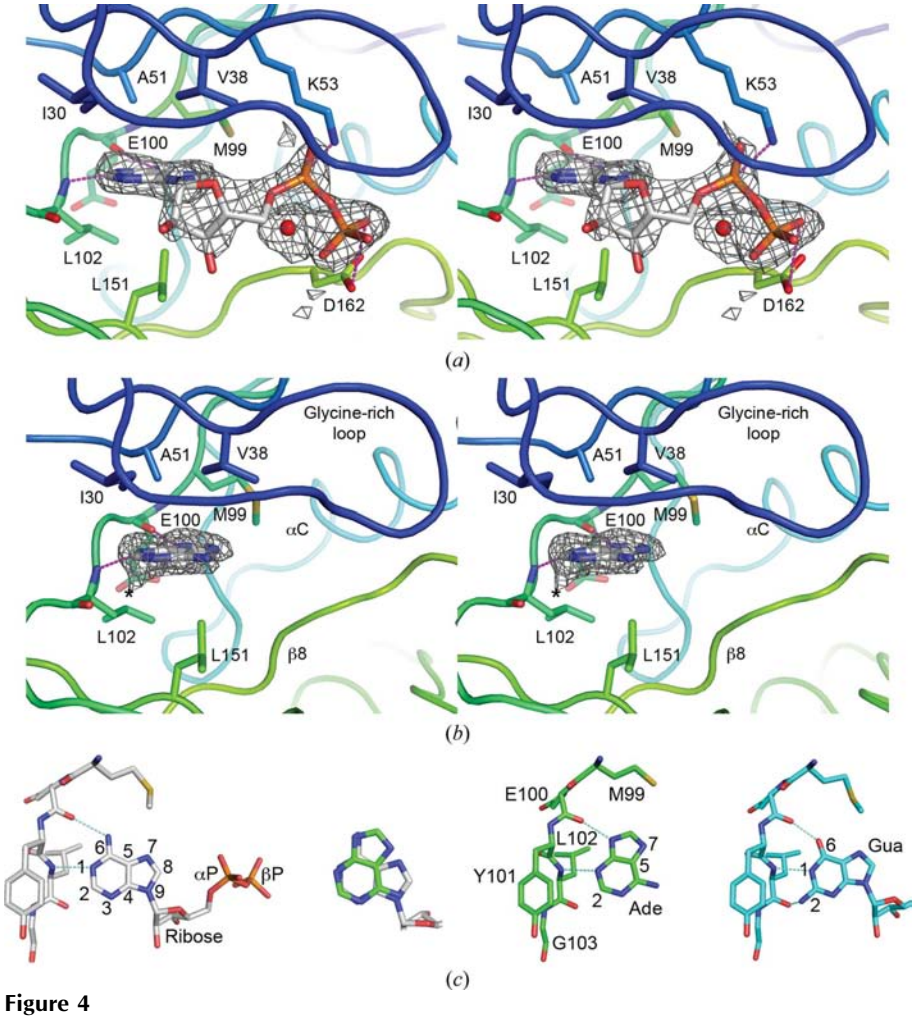

Figure 4
Interactions between MST3 and adenine. (*a*) The adenine base of the ADP bound to MST3(1–303) in the type II crystal forms hydrogen bonds (depicted as purple dashed lines) to the backbone atoms of Glu100 and Leu102 in the hinge region. It also interacts with nonpolar residues from both the N and C lobes of the enzyme. The sugar-phosphate moiety is not as well defined. The pyrophosphate may form hydrogen bonds to Lys53 and Asp162, but it may have an alternative conformation with its α-phosphate occupying the position of an adjacent water molecule (red sphere). (*b*) The free adenine in the type III crystal occupies a similar position, but is flipped over compared with that in (*a*). The asterisk marks the position of an attached atom to the purine ring which possibly arises from oxidation. The difference Fourier maps ($F_o - F_c$) shown here were calculated using refined models with the atoms in question omitted and are contoured at the 3σ level. (*c*) The different binding modes of adenine are compared in detail. The bound ADP in the type II crystal is shown on the left (with C atoms coloured white) and the adenosine in the type III crystal is shown in the centre (green C atoms). Their orientations differ by a 180° rotation about the C2—C5—N7 diagonal. A modelled guanosine (blue C atoms) based on the type III crystal structure of the MST3–Mn-ADP complex is shown on the far right. An additional hydrogen bond can be formed between N2 of guanine and the carbonyl O atom of Leu102.

Cocrystallization with Mg-ATP produced type III crystals, but the MST3(1–303) molecule did not bind to Mg^{2+} or ATP. Instead, a free adenine base was found in its active site, as suggested by clear electron density in difference Fourier maps (Fig. 4*b*). Surprisingly, the purine binds to the enzyme in an orientation that is distinct from that of the previous ADP complex. Although both rings occupy almost the same position, they deviate from each other by a flipping of the planar molecule about a line connecting C2 to C5 (or N7; Fig. 4*c*). The backbone O and N atoms of Glu100 and Leu102 form hydrogen bonds to N9 and N3 of the adenine, respectively, instead of N6 and N1 when the ligand is a nucleotide. The adenine may have arisen from some impurity in the ATP or from cleavage of the glycosidic bond of the nucleotide during crystallization (Tehrani *et al.*, 2009). Additionally, the electron density shows a small out-of-plane protrusion at C2, suggesting that it might have been partially oxidized and bear either a hydroxyl or an amino group which is directed toward the backbone O atom of Leu102 (Fig. 4*b*). The second mode of purine-base binding may help to explain the alternative use of GTP by MST3 as a phosphate donor in the kinase reaction (Schinkmann & Blenis, 1997).

3.4. The Mn-ADP complex

It has been noted since MST3 kinase was first cloned and characterized by Schinkmann & Blenis (1997) that the

enzyme not only uses both ATP and GTP but also has a preference for Mn^{2+} rather than Mg^{2+} as its metal-ion cofactor. Indeed, we were only able to obtain type III crystals of the ternary complex by including manganese acetate, along with ADP and $MgCl_2$, in the crystallization mother liquor. As shown in Fig. 5(*a*), the nucleotide and the metal ions in the active site have well defined electron densities, except for a break between the α- and β-phosphate groups. Although the β-phosphate has a somewhat higher B value of 36 Å^2, the average B value of these ligands is comparable to that of the protein (Table 1), suggesting that the Mn-ADP complex is more stable than the previous type II ADP complex crystal, presumably because the metal ions participate in the enzyme–ligand interactions. The refined B values of both Mn^{2+} ions are 32 Å^2 and the corresponding strong electron densities are consistent with their assignment as Mn^{2+} ions instead of Mg^{2+}. In this region, only the Pα atom (but not Pβ) of ADP has similarly strong density. One Mn^{2+} ion (Mn1) is coordinated to three water molecules, the α-phosphate group and the side chains of Asn149 and Asp162 (equivalent to Asn171 and Asp184 in PKA). The other Mn^{2+} (Mn2) is bound by four waters, as well as the β-phosphate and the side chain of Asp162. The side-chain N$^{\zeta}$ atom of Lys53 (Lys72 in PKA) forms a three-way bridge with both the α- and β-phosphate of ADP and Glu70 (Glu91 in PKA) from the C helix (Fig. 5*a*). The β-phosphate also forms a hydrogen bond to the backbone N atom of Ser34 in the glycine-rich loop and some other hydrogen bonds between ADP and the loop are also likely. These interactions have been observed in other structures, including PKA (Kim *et al.*, 2005).

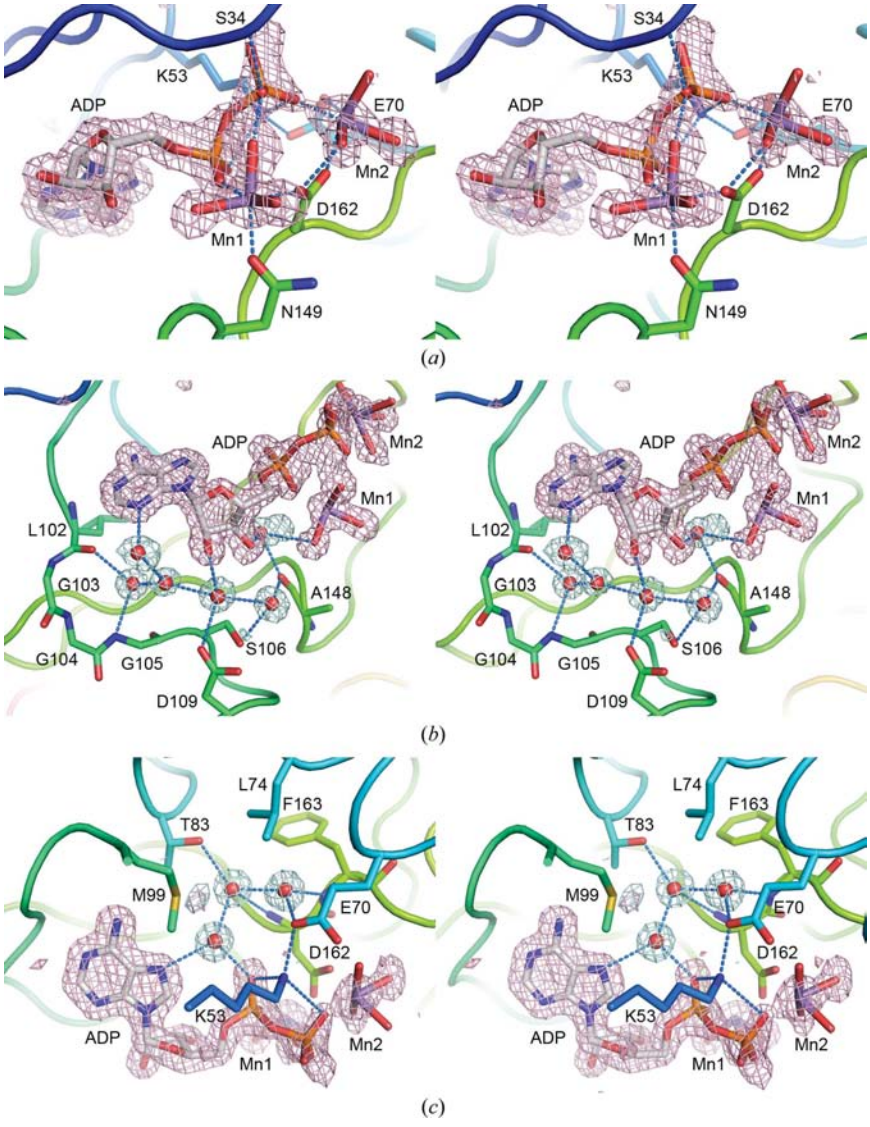

Figure 5
Interactions between MST3 and Mn-ADP. (*a*) The pyrophosphate moiety of ADP is bound by the backbone N atom of Ser34, the side chain of Lys53 and two Mn^{2+} ions. In addition to the pyrophosphate of ADP and the side chains of Glu70, Asn149 and Asp162, the Mn^{2+} ions are also bound to seven water molecules (three to Mn1 and four to Mn2), which are shown as stick models. Each Mn^{2+} ion has an octahedral configuration. The difference Fourier map ($F_o - F_c$) was calculated using the refined model with the relevant atoms omitted and is contoured in pink at the 3σ level. Those in (*b*) and (*c*) were calculated in the same way but are coloured cyan. Noncovalent bonds are shown as blue dashed lines. (*b*) Several well ordered water molecules form a hydrogen-bonding network with the adenosine moiety of ADP, which mediates its interaction with the enzyme, especially for the ribose part. (*c*) Three conserved waters are trapped in a pocket lined by nonpolar residues. The central role played by Lys53 is clear in this view. The density adjacent to Met99 S$^{\delta}$ may arise from alternate conformations of the methyl group or partial oxidation of the sulfur.

The structure of the adenosine moiety in the type III crystal of the Mn-ADP complex is virtually identical to that in the type II crystal of the ADP complex, in which the adenine forms hydrogen bonds to backbone atoms in the hinge and interacts with hydrophobic side chains from both the N and C lobes and the ribose appears not to interact directly with the protein. In contrast, the pyrophosphate moiety shows significant structural differences and, as described above, forms additional interactions with the enzyme. Moreover, the structure of the ribose moiety is much better defined in this crystal, as well as the positions of several water molecules that mediate the indirect protein–ligand interactions. Six water molecules form a hydrogen-bonding network which also involves the backbone atoms of the glycine-rich hinge and Ala148, the side chains of Ser106 and Asp109, the N3 of adenine and the two hydroxyl groups of the ribose as well as a water bound by the Mn1 ion (Fig. 5*b*). These waters have an average B value of 27 Å^2. On the other side, three waters (average B value of 20 Å^2) are trapped in a partly hydrophobic pocket lined by Leu74, Met99 and Phe163 and mediate hydrogen

bonds from the N7 of adenine and the α-phosphate to the protein (Fig. 5*c*). These three waters are also seen in the type II crystal of the MST3–ADP complex, although a water molecule is displaced by a slightly different side-chain conformation of Glu70 in one of the two complexes. However, the water molecules on the more open side of ADP are less conserved.

4. Discussion

4.1. Implications for activation mechanism

The C-terminal helix of MST3(1–303) spans the thickness of the C lobe. It contains at least 18 residues beginning at Lys280 and is approximately 30 Å long. If the opening of the ATP-binding pocket in the active-site cleft is said to be located at the front of the enzyme molecule, as seen in catalytic domain drawings of most protein kinases, the long helix propagates from the back to the front of the MST3 catalytic domain. Although the regulatory domain of MST3 is not present in the crystals studied here, it is most probably located in front of the catalytic domain and consequently renders the active site inaccessible to substrate and cofactor. Secondary-structural prediction based on the amino-acid sequence suggests that this 128-residue region is mostly α-helical. The regulatory domain of MST3 encompasses the region 400–420, which corresponds to a core segment 445–465 of coiled coil in the regulatory domain of MST1, which forms a dimer (Huang *et al.*, 2002; Hwang *et al.*, 2007). Expression of the MST3(1–303) T178A mutant in *E. coli* resulted in aggregated protein. Full-length MST3 also tended to form aggregates. Although the dimer formation of MST3 remains to be elucidated, these observations suggest that the activation loop and the C-terminal domain may somehow be related to the self-association of the enzyme.

The electron densities corresponding to pThr178 are weak in the type I and type II crystals, but analysis shows that this is because of flexibility rather than partial phosphorylation. In contrast, judging by its strong density and low *B* value, Thr178 is fully phosphorylated in the type III crystals, as in the case of PAKs (Eswaran *et al.*, 2007). Because of their similar structures, pThr178 can be mimicked by mutating it to Glu178. The MST3(1–303) T178E mutant has been crystallized in unit cells isomorphous to those of the type II and type III crystals of the wild-type protein (Table S1). If the activation of MST3 by phosphorylation occurs in an intramolecular manner, pre-treatment of the MST3(1–303) protein by incubation at 310 K with ATP and Mn^{2+} or Mg^{2+} ions would lead to the phosphorylation of most Thr178 residues and thus result in a uniform conformation of the activation loop. However, such a procedure did not improve the quality of the crystals, which were obtained almost exclusively in the type II unit cell and only diffracted X-rays to about 2 Å resolution (Table S1). It is possible that other Ser/Thr residues at less specific sites were phosphorylated by the already activated enzyme during the treatment, unexpectedly increasing the diversity of protein conformations.

4.2. Nucleotide and cofactor binding

A common feature of MST3(1–303) structures in complex with either adenosine or ADP is that the purine base forms two specific hydrogen bonds to the hinge, while the plane position of the base is well conserved. In fact, most kinase inhibitors contain a planar group that mimics the purine base and forms similar hydrogen bonds to the hinge (Noble *et al.*, 2004). The emergence of electron density for an additional atom from the adenine ring (near C2) towards the backbone O atom of Leu102 allows the construction of a model for bound guanosine (Figs. 4*b* and 4*c*). However, the guanine base should undergo tautomerization by a proton shift from N1 to O6 (Figure S2). This is a less common formation than in the conventional G–C base pairs of DNA, but it enables GTP to make one more specific hydrogen bond than the two original ATP hydrogen bonds. In the type II crystals, the ribose and the phosphate groups of the bound ADP are not as well defined as those in the type III crystals, but there are three conserved water molecules in a nonpolar pocket adjacent to the ribose (Fig. 5*c*). Exclusion of these waters by some hydrophobic group attached to a purine base may offer a starting point for drug design targeted at the MST-family protein kinases. Interestingly, the equivalent cavity in the kinase domain of Abl (an Abelson murine leukaemia oncogene homologue) is occupied by the third ring of the drug Gleevec (Noble *et al.*, 2004; see also PDB entry 3gvu; E. Salah, E. Ugochukwu, A. Barr, P. Mahajan, B. Shrestha, P. Savitsky & S. Knapp, unpublished work).

Incorporation of manganese acetate and ADP in the co-crystallization experiments produced ternary-complex crystals, in which the ribose and pyrophosphate moieties were both clearly seen. The octahedral coordination of the two Mn^{2+} ions by protein atoms, the pyrophosphate group and water molecules stabilizes complex formation, so the entire ADP molecule is bound tightly, as indicated by its low *B* value. Such ternary-complex crystals could be obtained using Mn^{2+}, but not with Mg^{2+} or Zn^{2+}. Although the mother liquor of each type II or type III crystal contained 150–200 m*M* $MgCl_2$, Mg^{2+} ion was never observed in the structures. In constrast, Mn^{2+} ions were observed when 5 m*M* manganese acetate was added. Using $ZnCl_2$ produced similar results as with $MgCl_2$. These results indicate specific binding of Mn^{2+} and are consistent with the requirement of Mn^{2+} ion as the metal cofactor of MST3, as previously elucidated (Lu *et al.*, 2006). The use of Mn^{2+} as a cofactor is less common in Ser/Thr kinases than in tyrosine kinases. Interestingly, in phosphorylase kinase Mn^{2+} facilitates the use of GTP as a phosphoryl-group donor (Graves *et al.*, 1999).

For MST3, binding of the nucleotide and cofactor does not seem to be correlated with the open–closed conformational changes in the catalytic domain. The rotations of up to 12° between the N lobe and the C lobe are more likely to be a result of their structural flexibility. Contrary to the frequent observation that substrate binding induces domain closure of an enzyme, the unliganded type I crystal structure represents the most closed conformation of the MST3 catalytic domain (Fig. 2). The conformation of the glycine-rich loop is especially

variable. Interestingly, it has a more open conformation in the Mn-ADP complex than in the adenine complex. This is not a result of crystal packing, since the crystals are isomorphous (both type III). Instead, the loop moves outwards to accommodate the bound pyrophosphate and metal ions. In general, the structures of the catalytic domain of protein kinases are more conserved than their regulatory mechanisms (Noble *et al.*, 2004). It would be desirable if a purine-derived or other inhibitor targeted at the active site of MST3 could also stabilize the interactions between the regulatory and catalytic domains in the full-length protein. Thus, the enzyme would remain inactive even after caspase cleavage.

The authors thank the National Synchrotron Radiation Research Center, Taiwan and SPring-8 and Photon Factory, Japan for beam-time allocations. This work was supported by Academia Sinica and a grant from the National Science Council of Taiwan (NSC-97-3112-B-001-017 to AH-JW).

References

Brünger, A. T., Adams, P. D., Clore, G. M., DeLano, W. L., Gros, P., Grosse-Kunstleve, R. W., Jiang, J.-S., Kuszewski, J., Nilges, M., Pannu, N. S., Read, R. J., Rice, L. M., Simonson, T. & Warren, G. L. (1998). *Acta Cryst.* D**54**, 905–921.

DeLano, W. L. (2008). *The PyMOL Molecular Viewer.* DeLano Scientific, Palo Alto, California, USA. http://www.pymol.org.

Eswaran, J., Lee, W. H., Debreczeni, J. É., Filippakopoulos, P., Turnbull, A., Fedorov, O., Deacon, S. W., Peterson, J. R. & Knapp, S. (2007). *Structure*, **15**, 201–213.

Goldsmith, E. J., Akella, R., Min, X., Zhou, T. & Humphreys, J. M. (2007). *Chem. Rev.* **107**, 5065–5081.

Graves, D., Bartleson, C., Biorn, A. & Pete, M. (1999). *Pharmacol. Ther.* **82**, 143–155.

Huang, C. Y., Wu, Y. M., Hsu, C. Y., Lee, W. S., Lai, M. D., Lu, T. J., Huang, C. L., Leu, T. H., Shih, H. M., Fang, H. I., Robinson, D. R., Kung, H. J. & Yuan, C. J. (2002). *J. Biol. Chem.* **277**, 34367–34374.

Hwang, E., Ryu, K. S., Pääkkönen, K., Güntert, P., Cheong, H. K., Lim, D. S., Lee, J. O., Jeon, Y. H. & Cheong, C. (2007). *Proc. Natl Acad. Sci. USA*, **104**, 9236–9241.

Johnson, D. A., Akamine, P., Radzio-Andzelm, E., Madhusudan & Taylor, S. S. (2001). *Chem. Rev.* **101**, 2243–2270.

Jones, T. A., Zou, J.-Y., Cowan, S. W. & Kjeldgaard, M. (1991). *Acta Cryst.* A**47**, 110–119.

Kim, C., Xuong, N.-H. & Taylor, S. S. (2005). *Science*, **307**, 690–696.

Lehtinen, M. K. & Bonni, A. (2008). *Curr. Mol. Med.* **8**, 313–318.

Lehtinen, M. K., Yuan, Z., Boag, P. R., Yang, Y., Villen, J., Becker, E. B. E., DiBacco, S., de la Iglesia, N., Gygi, S., Blackwell, T. K. & Bonni, A. (2006). *Cell*, **125**, 987–1001.

Lei, M., Lu, W., Meng, W., Parrini, M. C., Eck, M. J., Mayer, B. J. & Harrison, S. C. (2000). *Cell*, **102**, 387–397.

Lei, M., Robinson, M. A. & Harrison, S. C. (2005). *Structure*, **13**, 769–778.

Ling, P., Lu, T. J., Yuan, C. J. & Lai, M. D. (2008). *Cell. Signal.* **20**, 1237–1247.

Lu, T. J., Lai, W. Y., Huang, C. Y., Hsieh, W. J., Yu, J. S., Hsieh, Y. J., Chang, W. T., Leu, T. H., Chang, W. C., Chuang, W. J., Tang, M. J., Chen, T. Y., Lu, T. L. & Lai, M. D. (2006). *J. Biol. Chem.* **281**, 38405–38417.

McPherson, A. (1999). *Crystallization of Biological Macromolecules.* New York: Cold Spring Harbor Laboratory Press.

Min, X., Akella, R., He, H., Humphreys, J. M., Tsutakawa, S. E., Lee, S. J., Tainer, J. A., Cobb, M. H. & Goldsmith, E. J. (2009). *Structure*, **17**, 96–104.

Noble, M. E. M., Endicott, J. A. & Johnson, L. N. (2004). *Science*, **303**, 1800–1805.

Nolen, B., Taylor, S. & Ghosh, G. (2004). *Mol. Cell*, **15**, 661–675.

Ohren, J. F. *et al.* (2004). *Nature Struct. Mol. Biol.* **11**, 1192–1197.

Oliver, A. W., Knapp, S. & Pearl, L. H. (2007). *Trends Biochem. Sci.* **32**, 351–356.

Otwinowski, Z. & Minor, W. (1997). *Methods Enzymol.* **276**, 307–326.

Pike, A. C. W., Rellos, P., Niesen, F. H., Turnbull, A., Oliver, A. W., Parker, S. A., Turk, B. E., Pearl, L. H. & Knapp, S. (2008). *EMBO J.* **27**, 704–714.

Richardson, J. S. (1981). *Adv. Protein Chem.* **34**, 167–339.

Schinkmann, K. & Blenis, J. (1997). *J. Biol. Chem.* **272**, 28695–28703.

Tehrani, Z. A., Fattahi, A. & Pourjavadi, A. (2009). *Carbohydr Res.* **344**, 771–778.